Stripe motion artifact suppression in phase-resolved OCT blood flow images of the human eye based on the frequency rejection filter

Guozhong Liu (刘国忠)[1*] **and Ruikang Wang (王瑞康)**[2]

[1]*School of Instrument Science and Opto-Electronics Engineering, Beijing Information Science and Technology University, Beijing 100192, China*

[2]*Department of Bioengineering, University of Washington, 3720 15th Avenue Northeast, Seattle, Washington 98195, USA*

[*]*Corresponding author: liuguozhong@bistu.edu.cn*

Stripe motion artifacts caused by phase fluctuation in phase-resolved optical coherence tomography (OCT) result in the quality degradation of the image of *in vivo* blood flow of human eye. In order to suppress the stripe motion artifacts, we design a kind of frequency rejection filter aimed at the frequency spectrum characteristics of the image. Blood flow images of human eye acquired by our research group and another group are filtered to show the performance of the proposed method. Experimental results indicate that the stripe motion artifacts in the projection images are rejected significantly with minimal loss of signal information. The proposed filter can also be used in other imaging systems with similar stripe noise.

OCIS codes: 170.5755, 170.4500, 100.3008.

doi: 10.3788/COL201311.031701.

Optical coherence tomography (OCT)[1,2] has become an increasingly important imaging technique for diagnostic applications and biomedical research, enabling the visualization of the internal structure of tissue *in vivo* with micron scale resolution. As an example, OCT can image the retina and quantitatively measure changes in the retinal nerve fiber layer thickness, enabling the diagnosis of glaucoma as well as the assessment of progression and response to therapy[3]. In addition to the imaging of the micro-structural features of the sample, OCT development has further evolved into phase-resolved technology, which can image *in vivo* blood flow in tissue by evaluating the phase information between adjacent A-line scans or B-scans[4−6] to aid the diagnosis and treatment for clinicians and physicians[7,8]. Although OCT acquisition speeds of up to 1.37 million A-scans per second have been demonstrated for retinal imaging[9], motion artifacts caused by the galvanometer positioning accuracy, system mechanical jitter, and especially the movement of the sample still exist for *in vivo* three-dimensional (3D) imaging of the human eye[10]. The motion artifacts lead to the distortion of the tissue structure image and the blood flow image within tissue beds, which may adversely affect image interpretation and analyze as well as limit the performance of OCT for ophthalmic *in vivo* imaging.

There have been many efforts to solve the motion artifact problem in structural OCT imaging. Software algorithm[10−13] based on A-scan, B-scan, or 3D volume data and methods based on additional hardware[14−16] have been used to compensate for axial motion or/and transverse motion. A number of hardware[17,18] and post-processing methods[19−21] have also been investigated to overcome the phase stable problem of the phase-resolved OCT. Given that the phase of the OCT signal is very sensitive to the movement between device and sample, *in vivo* blood flow imaging of human eye still shows residual stripe motion artifacts.

In this letter, we propose a kind of frequency rejection filter aimed at the frequency spectrum characteristics of the image in order to eliminate the stripe motion artifacts. We then demonstrate the effectiveness of the proposed method using *en face* images and intensity projection images of the 3D blood flow volume data of human eye.

The OCT system used to acquire blood flow image of human retina and choroids is shown in Fig. 1, which is similar to a previously reported system[21]. The system used in this letter employed a super luminescent diode light source, with a central wavelength of 842 nm and provided a ∼8-μm axial resolution. The light was split into two paths in a fiber-based Michelson interferometer. One beam was coupled onto a stationary reference mirror, and the second beam was focused with a collimating lens, an objective lens, and an ocular lens at the posterior part of the eye with a theoretical lateral resolution of ∼16 μm. The focal spot on the sample was scanned using a pair of galvanometer mirror mounted in the sample
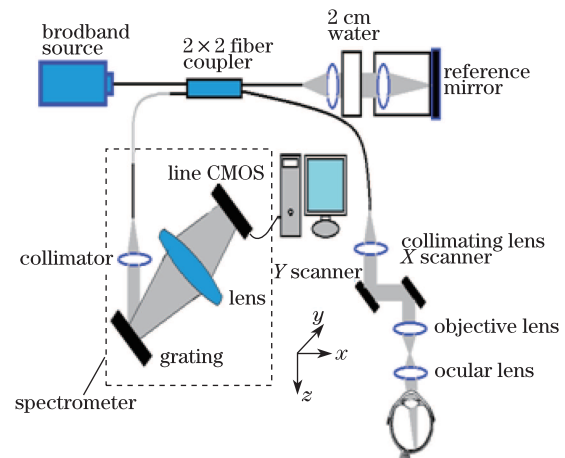

Fig. 1. Schematic of the OCT system.

arm. The light returning from the reference arm and the sample arm was sent to a homebuilt spectrometer, consisting of a 30-mm focal length collimator, a diffracting grating (1 200 lines/mm), an achromatic focusing lens with a 150-mm focal length and 1 024 element linear array CCD detector. A 2-cm water chamber was used in the reference arm to pre-compensate the wavelength dispersion effect caused by the human eye.

The scanning pattern and method for processing the acquired data were based on an optical microangiography (OMAG) technique[22]. This technique allows the extraction of the 3D microvascular images. Briefly, in order to acquire original 3D volume data, we used two galvo-scanners (X scanner and Y scanner as displayed in Fig. 1) to raster-scan the focused beam spot across the sample with a scanning area of 2.5×2.0 (mm). A saw tooth waveform was used to drive the X scanner (for fast B-scan), and a step function waveform was used to drive the Y scanner (for slow C-scan). For a B-scan cross-sectional image, 500 A-lines were captured with ~ 5-μm spatial interval between adjacent A-lines. For the C-scan, the 2-mm scan range was evenly divided into 200 steps with a 10-μm spatial interval between them. In each step, five B-scan frames were captured and processed to extract one B-scan cross-sectional flow image. Each nonlinear spectral interferogram that represented an A-scan was rescaled into linear k-space followed by fast Fourier transform (FFT) to become A-line complex OCT signals (phase and amplitude) along the z axis. This can be written as

$$F(x, z) = A(x, z)\exp[\mathrm{i}\varphi(x, z)], \qquad (1)$$

where $A(x, z)$ and $\varphi(x, z)$ are the amplitude and the phase of $F(x, z)$, respectively, x is the lateral position of the probe beam, and z represents the coordinates along the imaging depth. In our system, the phase differences between adjacent A-lines of two B-scans in the same C-scan position can be expressed as

$$\Delta\varphi(x, z) = \Delta\varphi_{\mathrm{BF}}(x, z) + \Delta\varphi_{\mathrm{M}}(x, z) + \Delta\varphi_{\mathrm{N}}, \qquad (2)$$

where $\Delta\varphi_{\mathrm{BF}}(x, z)$ is the phase term caused by the moving red blood cells, $\Delta\varphi_{\mathrm{M}}(x, z)$ is the phase term caused by the subject bulk motion, and $\Delta\varphi_{\mathrm{N}}$ is the random phase noise. The B-scan cross-sectional blood flow image were acquired when the bulk motion term $\Delta\varphi_{\mathrm{M}}(x, z)$ were eliminated through the application of a phase compensation method based on histogram estimation[22]. Five B-scan images acquired in the same C-scan position were used to produce four B-scan blood flow images, and these were averaged to improve the blood flow image quality.

Typical B-scan amplitude and phase images are shown in Figs. 2(a) and (b), respectively. Figures 2(c) and (d) are the respective B-Scan cross-sectional blood flow images acquired at different C-Scan positions. Figure 2(c) shows a clear blood flow map with minimal noise. Although the bulk motion phase compensation is performed, there is much phase fluctuation noise in the blood flow image in Fig. 2(d) owing to the phase fluctuation between adjacent A lines of B-Scans acquired at the same position of Y-scanner. Figure 2(e) shows an *en face* intensity projection image $i(x, y)$ of 3D blood flow volume data of human eye, which can provide blood flow

map within microcirculation tissue beds. However, the stripe motion artifacts along the fast scanning direction produced by the phase fluctuation noise (Fig. 2(d)) seriously deteriorate the image quality.

Figure 2(f) shows the logarithmic amplitude spectrum $I(u, v)$ of the *en face* intensity projection image $i(x, y)$ in Fig. 2(e). As we noticed from the spectrum, the frequency components in the rectangular area encompassing frequency axis $u = 0$ have very high intensity, which are related to the stripe motion artifacts along the fast scanning direction (x direction) in the spatial domain. However, these frequency components cannot be removed
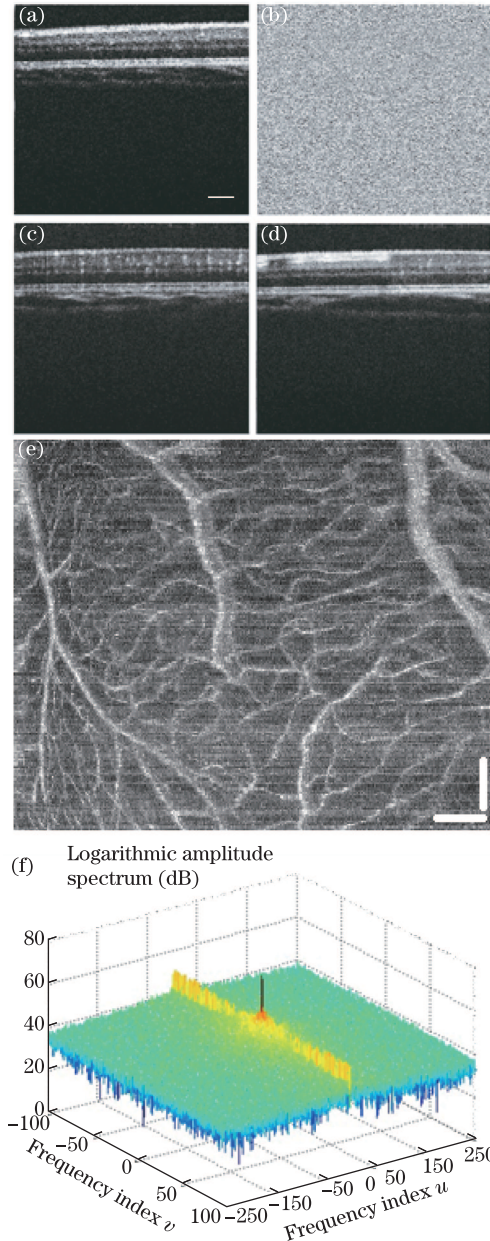

Fig. 2. Acquiring of *en face* intensity projection image of 3D blood flow volume data of human eye in OCT. Typical B-scan (a) amplitude image and (b) phase images, respectively; typical B-scan blood flow image with (c) little and (d) much phase fluctuation noise; (e) *en face* intensity projection image of 3D blood flow volume data of human eye; (f) frequency spectrum of (e). Scale bars are 250 μm.
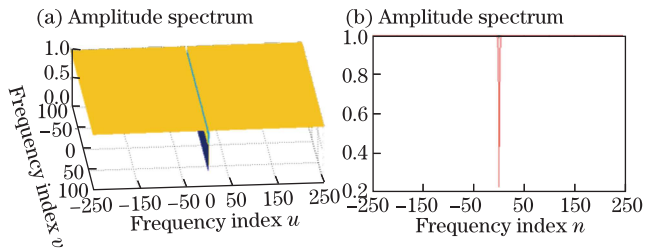
Fig. 3. Illustration of the frequency spectrum of the designed frequency rejection filter in the case of (a) 3D and (b) 2D displays along the frequency u direction.

completely, because they are also related to the useful signal information of the image. Therefore, according to the frequency spectrum characteristics of the image, including stripe motion artifacts, we design a kind of frequency rejection filter to eliminate the stripe motion artifacts in the blood flow image while preserving the useful signal information.

The transfer function $F(u, v)$ of the frequency rejection filter is expressed as

$$F(u, v) = 1 - e^{-\alpha(|u|+1)^2}, \tag{3}$$

where u and v are the frequency axes, respectively, and α is the filter rejection factor. We can obtain the relationship from Eq. (3), that is, the lower the rejection factor α is, the higher the suppression degree required to stripe motion artifacts. If a large factor α is selected, the stripe motion artifacts could not be removed completely. Inversely, if the factor α is too small, the stripe motion artifacts are removed and the signal information in the image is reduced. Figure 3(a) shows the amplitude frequency spectrum of the filter when the factor α is 0.47 and Fig. 3(b) is the 2D display along the frequency u direction shown in Fig. 3(a).

The filtered frequency spectrum of blood flow image is expressed as

$$I'(u, v) = I(u, v) \cdot F(u, v). \tag{4}$$

The filtered image with minimal stripe motion artifacts acquired by inverse FFT can be obtained using

$$i'(x, y) = F^{-1}[I'(u, v)]. \tag{5}$$

Figure 4(a) shows the filtered result of the original blood flow image (Fig. 2(e)) when the filter factor $\alpha = 0.35$. It can be observed that the stripe motion artifacts are almost rejected and the blood flow map within the retina is displayed clearly. Figure 4(b) shows the amplitude frequency spectrum of Fig. 4(a), indicating that the frequency components related to the stripe motion artifacts are suppressed appropriately. In order to further demonstrate the effectiveness of the designed filter, we plotted the gray value of the line marked A in Fig. 4(a) before filtering (Fig. 5(a)) and after filtering (Fig. 5(b)). The red horizontal straight lines in Fig. 5(a) and the blue horizontal straight lines in Fig. 5(b) display the intensity of the stripe motion artifacts before filtering and after filtering, respectively. Comparing Figs. 5(a) and (b), the stripe motion artifacts is substantially rejected and the signal-to-noise ratio (SNR) of the blood flow image is improved.

Figure 6(a) shows an *en face* intensity projection image of the inner retinal layer acquired with a 1 050-nm swept source OCT system by Schmoll *et al.*[23] and Fig. 6(b) shows the filtered result of Fig. 6(a) when filter factor $\alpha = 0.4$. The stripe motion artifacts in Fig. 6(a) is also removed effectively.

Figure 7 illustrates the change of the filter results of an *en face* blood flow image with the filter rejection factor α. The blood flow signal information may be partially removed (e.g., Figs. 7(b) and (c)) or the stripe motion artifacts cannot be rejected completely (e.g., Fig. 7(e) and (f)) when the factor α is not selected correctly. When the factor α is 0.3 (Fig. 7(d)), the stripe motion artifacts is suppressed effectively with minimal loss of blood flow signal information.

The filtered results of an *en face* blood flow image using proposed frequency rejection filter and other filter techniques are compared in Fig. 8. Figure 8(b) shows the filtered result of Fig. 8(a) using DC removal through
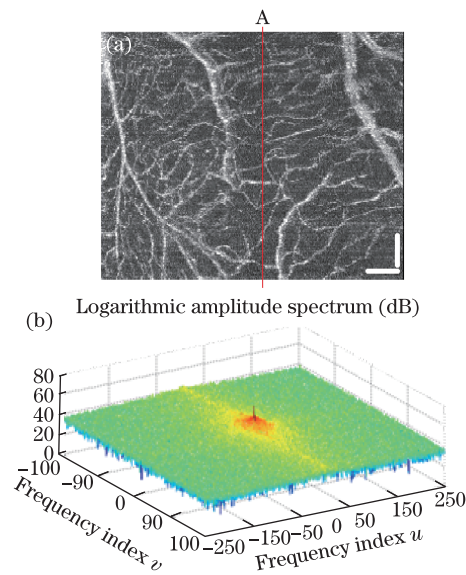

Fig. 4. (a) Filtered image of Fig. 2(e); (b) amplitude frequency spectrum of (a). Scale bars are 250 μm.
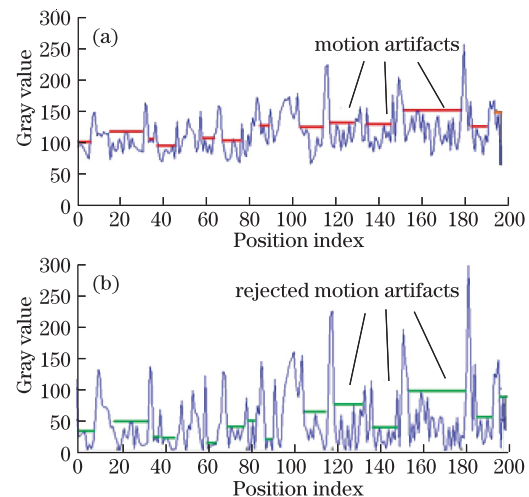

Fig. 5. (Color online) Illustration of the filter performance by plotting the gray value of the line marked A in Fig. 4(a) in case of (a) before and (b) after filtering.
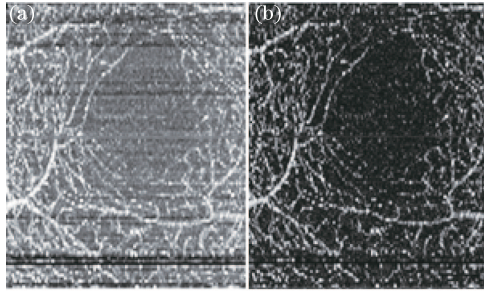
Fig. 6. Illustration of the filter performance by comparing the en face projection image of human eye copied from one reference in the case of (a) before and (b) after filtering.
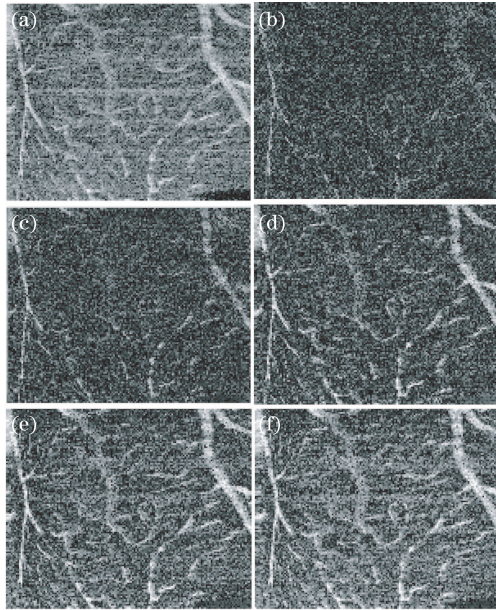

Fig. 7. Illustration of the filter results of (a) an *en face* blood flow image when filter factor (b) $\alpha = 0.01$, (c) $\alpha = 0.05$, (d) $\alpha = 0.3$, (e) $\alpha = 0.7$, and (f) $\alpha = 1$, respectively.
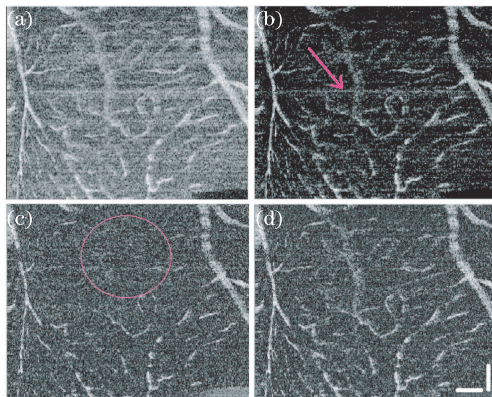

Fig. 8. Comparison of the filtered results of (a) an en face blood flow image using (b) DC removal through background subtraction filter (c) high pass filter (DC removal) in the fast scanning direction, and (d) proposed frequency rejection filter, respectively. Scale bars are 250 μm.

background subtraction method, in which the stripe motion artifacts still exists as indicated by the red arrow. Figure 8(c) shows the filtered result of Fig. 8(a) using the high pass filter with very low cut off frequency (DC

removal) in the fast scanning direction. The blood flow signal information in the area indicated by the red circle is also removed by the filter, while suppressing the stripe motion artifacts. Obviously, the proposed frequency rejection filter can suppress the stripe motion artifacts effectively while preserving the blood flow signal information.

As a general rule, blood vessels branch in all directions, therefore, the rejection of the stripe motion artifacts along the fast scanning direction (x direction) by frequency rejection filter does not lead to the obvious loss of blood flow information. When large amounts of blood vessels are distributed in the similar direction (x direction) with the stripe motion artifacts, they have similar frequency components with the stripe motion artifacts in the frequency domain, leading to the loss of blood flow signal information when frequency rejection filter is used to remove the stripe motion artifacts. In this case, the sample must be scanned again with different scanning directions.

In conclusion, we design a frequency rejection filter model aimed at the frequency spectrum characteristics of the blood flow image in OCT. This model is used to remove the stripe motion artifacts caused by the galvanometer positioning accuracy, system mechanical jitter, and the movement of the sample. We demonstrate that the stripe motion artifacts in the blood flow image can be removed with a minimal loss of signal information. Furthermore, the SNR of the blood flow image can be obviously improved, which is very important in disease diagnosis and research based on blood flow map. Although a spectrometer-based OCT system is considered, the proposed method is also applicable to swept-source OCT system, full-field OCT system, and other raster-scan imaging system with similar stripe noise. The technique can also suppress stripe noise in any direction of the image after the filter is appropriately revised.

References

1. D. Huang, E. A. Swanson, C. P. Lin, J. S. Schuman, W. G. Stinson, W. Chang, M. R. Hee, T. Flotte, K. Gregory, C. A. Pauliafito, and J. G. Fujimoto, Science **254**, 1178 (1991).
2. A. F. Fercher, W. Drexler, C. K. Hitzenberger, and T. Lasser, Rep. Prog. Phys. **66**, 239 (2003).
3. J. S. Schuman, C. A. Puliafito, and J. G. Fujimoto, *Optical Coherence Tomography of Ocular Diseases*, 2nd ed. (Slack, Thorofare, 2004).
4. Y. Zhao, Z. Chen, C. Saxer, S. Xiang, J. F. de Boer, and J. S. Nelson, Opt. Lett. **25**, 114 (2005).
5. J. Zhang and Z. P. Chen, Opt. Express **13**, 7449 (2005).
6. R. K. Wang, S. L. Jacques, Z. H. Ma, S. Hanson, and A. Gruber, Opt. Express **15**, 4083 (2007).
7. R. A. Leitgeb, L. Schmetterer, W. Drexler, A. F. Fercher, R. J. Zawadzki, and T. Bajraszewski, Opt. Express **11**, 3116 (2003).
8. B. J. Vakoc, S. H. Yun, J. F. de Boer, G. J. Tearney, and

    B. E. Bouma, Opt. Express **13,** 5483 (2005).

9. S. Ricco, M. Chen, H. Ishikawa, G. Wollstein, and J. Schuman, in *Proceedings of Medical Image Computing and Computer-Assisted Intervention*2009 100 (2009).

10. M. F. Kraus, B. Potsaid, M. A. Mayer, R. Bock, B. Baumann, J. J. Liu, J. Hornegger, and J. G. Fujimoto, Biomed. Opt. Express **3,** 1182 (2012).

11. E. A. Swanson, J. A. Izatt, M. R. Hee, D. Huang, C. P. Lin, J. S. Schuman, C. A. Puliafito, and J. G. Fujimoto, Opt. Lett. **18,** 1864 (1993).

12. R. J. Zawadzki, A. R. Fuller, S. S. Choi, D. F. Wiley, B. Hamann, and J. S. Werner, Proc. SPIE **6426,** 642607 (2007).

13. T. M. Jørgensen and B. Sander, Proc. SPIE **6426,** 642608 (2007).

14. R. D. Ferguson, D. X. Hammer, L. A. Paunescu, S. Beaton, and J. S. Schuman, Opt. Lett. **29,** 2139 (2004).

15. D. X. Hammer, R. D. Ferguson, J. C. Magill, L. A. Paunescu, S. Beaton, H. Ishikawa, G. Wollstein, and J.

S. Schuman, J. Biomed. Opt. **10,** 024038 (2005).

16. D. Sacchet, M. Brzezinski, J. Moreau, P. Georges, and A. Dubois, Appl. Opt. **49,** 1480 (2010).

17. D. Lin, X. Jiang, F. Xie, W. Zhang, L. Zhang, and I. Bennion, Opt. Express **12,** 5729 (2004).

18. Z. Yaqoob, W. Choi, S. Oh, N. Lue, Y. Park, C. Fang-Yen, R. R. Dasari, K. Badizadegan, and M. S. Feld, Opt. Express **17,** 10681 (2009).

19. P. H. Tomlins and R. K. Wang, Meas. Sci. Technol. **18,** 3365 (2007).

20. T. S. Ralston, D. L. Marks, P. S. Carney, and S. A. Boppart, in *Proceedings of 3rd IEEE International Symposium on Biomedical Imaging: Nano to Macro* 578 (2006).

21. L. An and R. K. Wang, Opt. Express **16,** 11438 (2008).

22. L. An, J. Qin, and R. K. Wang, Opt. Express **18,** 8220 (2010).

23. T. Schmoll, A. S. G. Singh, C. Blatter, S. Schriefl, C. Ahlers, U. Schmidt-Erfurth, and R. A. Leitgeb, Biomed. Opt. Express **2,** 1159 (2011).